Toward the Large-Eddy Simulation Over a Hypersonic Elliptical Cross-Section Cone

M. Pino Martín[†]
Greg Weirs[‡]
Graham V. Candler[¶]
Ugo Piomelli[§]
Heath Johnson[†]
Ioannis Nompelis[*]

Abstract

A formulation of mixed subgrid-scale (SGS) models (i.e. models combining scale-similar and eddy viscosity contributions) for compressible flows in generalized curvilinear coordinates is presented and validated against a direct numerical simulation (DNS) database of a supersonic, zero-pressure gradient boundary layer. Also, the computational setup for the large-eddy simulation (LES) of a hypersonic elliptical cross-section cone is discussed in detail.

Introduction

The aerodynamic heating effects in hypersonic lifting bodies are significantly affected by transition and turbulence. A realistic representation of a lifting body is generally more complex than perfect gas flow over a flat plate and may include pressure gradients, streamline curvature, three-dimensional mean flow, separation, shocks, and chemical reactions. In the absence of detailed experimental or computational databases to better understand these physical phenomena, we are left with excessive design conservatism and unrefined conceptual designs.

When investigating these phenomena via CFD, direct numerical simulations are simply not affordable. However, recent advances in turbulence modeling provide a wide range of accuracy for simulating turbulent flows of engineering interest. Depending on the level of detail required, one may chose the simple Reynolds-averaged Navier-Stokes models or the state of the art subgrid scale models in a large-eddy simulation to obtain a more refined prediction. Clearly the study of fundamental physical phenomena must be done using the finest possible method, namely LES. However, one must keep in mind that a key feature of the prediction is validation with experiments.

The highly three-dimensional character of the flows of interest presents a challenge for traditional measurement techniques. Using the most recent laser and camera technologies, Huntley *et al.*[1] present the first detailed flow visualization of transition on an elliptical cross-section cone at Mach 8. They use the experimental database to gain insight into the effect of three-dimensionality on the transition characteristics. Mean flow features and details about the unstable modes in the boundary layer for the same configuration are given by Kimmel *et al.*[2,3] and Poggie *et al.*,[4] respectively. Because this flow is being extensively documented experimentally and because the geometric configuration resembles that of the forebody of a hypersonic vehicle, we chose it to test state of the art SGS models for high speed flows.

The present work is an ongoing effort to provide detailed flow simulations of unsteady, hypersonic, transitional or turbulent flows. As a first step, we follow the recent work of Jordan[5] by transforming the DNS equations into a generalized curvilinear coordinate system and then filtering the equations to yield the LES equations in curvilinear coordinates. In this paper the conservative form of the DNS and LES equations in curvilinear grids are presented, the mixed SGS models used to represent the contribution of the unresolved turbulent scales along the curvilinear grid lines are listed, and the numerical method and filtering operations required to perform the simulations are exposed. The implementation of the LES in a generalized coordinate system is validated against the DNS database of a supersonic, zero-pressure gradient boundary layer. The grid requirements and initialization for the LES of a hypersonic, elliptical cross-section cone discussed

[†] Postdoctoral Fellow, Aerospace Engineering & Mechanics, University of Minnesota, Member AIAA (pino@aem.umn.edu)
[‡] Research Associate, ASCI Flash Center, University of Chicago, Member AIAA
[¶] Professor, Aerospace Engineering & Mechanics, University of Minnesota, Senior Member AIAA
[§] Professor, Mechanical Engineering, University of Maryland, Senior Member AIAA
[*] Graduate Student, Aerospace Engineering & Mechanics, University of Minnesota, Member AIAA

in detail. Finally a brief discussion about the ongoing work and the experimental data desirable for comparison with the computational simulations is given.

Governing equations

The equations describing the unsteady motion of a perfect gas flow are given by the mass, mass-averaged momentum, and total energy conservation equations

$$\frac{\partial \rho}{\partial t} + \frac{\partial}{\partial x_j}(\rho u_j) = 0,$$

$$\frac{\partial \rho u_i}{\partial t} + \frac{\partial}{\partial x_j}(\rho u_i u_j + p\delta_{ij} - \sigma_{ij}) = 0, \qquad (1)$$

$$\frac{\partial \rho e}{\partial t} + \frac{\partial}{\partial x_j}\Big((\rho e + p)u_j - u_i\sigma_{ij} + q_j\Big) = 0,$$

where ρ is the density, u_j is the velocity in the j direction, p is the pressure, σ_{ij} is the shear stress tensor given by a linear stress-strain relationship

$$\sigma_{ij} = 2\mu S_{ij} - \frac{2}{3}\mu\delta_{ij}S_{kk}, \qquad (2)$$

where $S_{ij} = \frac{1}{2}(\partial u_i/\partial x_j + \partial u_j/\partial x_i)$ is the strain rate tensor, and μ is the temperature dependent kinematic viscosity, q_j is the heat flux due to temperature gradients

$$q_j = -\kappa\frac{\partial T}{\partial x_j}\ , \qquad (3)$$

where κ is the temperature dependent thermal conductivity, and e is the total energy per unit mass given by

$$e = c_v T + \tfrac{1}{2}u_i u_i, \qquad (4)$$

where c_v is the specific heat at constant volume.

The governing equations can be implemented in a general curvilinear system using the transformation

$$\begin{pmatrix} \frac{\partial}{\partial x} \\ \frac{\partial}{\partial y} \\ \frac{\partial}{\partial z} \end{pmatrix} = \begin{pmatrix} \xi_x & \eta_x & \zeta_x \\ \xi_y & \eta_y & \zeta_y \\ \xi_z & \eta_z & \zeta_z \end{pmatrix} \begin{pmatrix} \frac{\partial}{\partial \xi} \\ \frac{\partial}{\partial \eta} \\ \frac{\partial}{\partial \zeta} \end{pmatrix}, \qquad (5)$$

where ξ is defined as the body-tangential in the streamwise direction, η the body-tangential in the spanwise direction, and ζ is the body-normal direction. Thus, the governing equations can be written in conservation form as

$$\frac{\partial U}{\partial t} + \frac{\partial F}{\partial \xi} + \frac{\partial G}{\partial \eta} + \frac{\partial H}{\partial \zeta} = 0, \qquad (7)$$

where U is the vector of conserved quantities, and F, G and H are the flux vectors in the ξ, η and ζ directions,respectively. Details of this transformation can be found in Hirsch.[6] The resulting flux vectors can be separated into their convective and viscous parts according to

$$F = F_c + F_v, \quad G = G_c + G_v \quad H = H_c + H_v. \qquad (8)$$

These vectors have the following form

$$U = J\begin{pmatrix} \rho \\ \rho u \\ \rho v \\ \rho w \\ \rho e \end{pmatrix}, \quad F = Jr_\xi \begin{pmatrix} \rho u' \\ \rho u u' + p s_x \\ \rho v u' + p s_y \\ \rho w u' + p s_z \\ (\rho e + p)u' \end{pmatrix},$$

$$F_v = -\,J\,r_\xi \begin{pmatrix} 0 \\ \sigma_{xx}s_x + \sigma_{xy}s_y + \sigma_{xz}s_z \\ \sigma_{yx}s_x + \sigma_{yy}s_y + \sigma_{yz}s_z \\ \sigma_{zx}s_x + \sigma_{zy}s_y + \sigma_{zz}s_z \\ (\sigma_{xx}u + \sigma_{xy}v + \sigma_{xz}w)s_x + \\ (\sigma_{yx}u + \sigma_{yy}v + \sigma_{yz}w)s_y + \\ (\sigma_{zx}u + \sigma_{zy}v + \sigma_{zz}w)s_z - \\ q_x s_x - q_y s_y - q_z s_z \end{pmatrix}, \qquad (9)$$

where s_x, s_y and s_z are the local direction cosines of the curvilinear coordinate system, namely for Eq. (9)

$$s_x = \xi_x/r_\xi\ , \quad s_y = \xi_y/r_\xi\ , \quad s_z = \xi_z/r_\xi\ , \qquad (10)$$

where $r_\xi = \sqrt{\xi_x^2 + \xi_y^2 + \xi_z^2}$ and u' is the velocity component in the body-tangential direction, namely for Equations (9)-(10)

$$u' = u s_x + v s_y + w s_z \qquad (11)$$

In this curvilinear coordinate system F, G and H are functionally equivalent. Thus, Equations (9) through (11) apply in the particular curvilinear direction.

Conserved LES equations

LES is based on the definition of a filtering operation: a resolved variable, denoted by an overbar, is defined as[7]

$$\overline{f}(\xi) = \int_D f(\xi')G(\xi, \xi'; \overline{\Delta})d\xi', \qquad (12)$$

where D is the entire domain, G is the filter function, and $\overline{\Delta}$ is the filter-width associated with the wavelength of the smallest scale retained by the filtering operation. Thus, the filter function determines the size and structure of the small scales. Jordan[5] shows that the filtering and differentiation operations commute in the curvilinear coordinate system if the numerical representation of the filtering operation has compact support. Therefore the LES form of the governing equations is given by

$$\frac{\partial \overline{U}}{\partial t} + \frac{\partial \overline{F}}{\partial \xi} + \frac{\partial \overline{G}}{\partial \eta} + \frac{\partial \overline{H}}{\partial \zeta} = \frac{\partial F_{\rm SGS}}{\partial \xi} + \frac{\partial G_{\rm SGS}}{\partial \eta} + \frac{\partial H_{\rm SGS}}{\partial \zeta}, \qquad (13)$$

where the flux and SGS vectors are functionally equivalent. To avoid the introduction of extra subgrid-scale terms in the equation of conservation of mass, it is convenient to use Favre-filtering.[8,9] A Favre-filtered variable is defined as $\widetilde{f} = \overline{\rho f}/\overline{\rho}$. Using the Favre-filtering definition the vectors in Eq. (13) can be written as

$$U = J \begin{pmatrix} \overline{\rho} \\ \overline{\rho}\,\widetilde{u} \\ \overline{\rho}\,\widetilde{v} \\ \overline{\rho}\,\widetilde{w} \\ \overline{\rho}\,\widetilde{e} \end{pmatrix}, \quad F = J r_\xi \begin{pmatrix} \overline{\rho}\,\widetilde{u}' \\ \overline{\rho}\,\widetilde{u}\widetilde{u}' + \overline{p} s_x \\ \overline{\rho}\,\widetilde{v}\widetilde{u}' + \overline{p} s_y \\ \overline{\rho}\,\widetilde{w}\widetilde{u}' + \overline{p} s_z \\ (\overline{\rho}\,\widetilde{e} + \overline{p})\widetilde{u}' \end{pmatrix},$$

$$F_v = - J r_\xi \begin{pmatrix} 0 \\ \widetilde{\sigma}_{xx} s_x + \widetilde{\sigma}_{xy} s_y + \widetilde{\sigma}_{xz} s_z \\ \widetilde{\sigma}_{yx} s_x + \widetilde{\sigma}_{yy} s_y + \widetilde{\sigma}_{yz} s_z \\ \widetilde{\sigma}_{zx} s_x + \widetilde{\sigma}_{zy} s_y + \widetilde{\sigma}_{zz} s_z \\ (\widetilde{\sigma}_{xx}\widetilde{u} + \widetilde{\sigma}_{xy}\widetilde{v} + \widetilde{\sigma}_{xz}\widetilde{w}) s_x + \\ (\widetilde{\sigma}_{yx}\widetilde{u} + \widetilde{\sigma}_{yy}\widetilde{v} + \widetilde{\sigma}_{yz}\widetilde{w}) s_y + \\ (\widetilde{\sigma}_{zx}\widetilde{u} + \widetilde{\sigma}_{zy}\widetilde{v} + \widetilde{\sigma}_{zz}\widetilde{w}) s_z - \\ \widetilde{q}_x s_x - \widetilde{q}_y s_y - \widetilde{q}_z s_z \end{pmatrix}, \quad (14)$$

$$F_{\mathrm{SGS}} = - J r_\xi \begin{pmatrix} 0 \\ \overline{\rho}\,(\widetilde{uu'} - \widetilde{u}\widetilde{u}') \\ \overline{\rho}\,(\widetilde{vu'} - \widetilde{v}\widetilde{u}') \\ \overline{\rho}\,(\widetilde{wu'} - \widetilde{w}\widetilde{u}') \\ \gamma c_v Q + \frac{1}{2}\mathcal{J} \end{pmatrix},$$

where the filtered energy is given by

$$\widetilde{e} = c_v \widetilde{T} + \frac{1}{2}\widetilde{u}_i\widetilde{u}_i + \frac{1}{2}(\widetilde{u_i u_i} - \widetilde{u}_i\widetilde{u}_i) \ , \quad (15)$$

and the SGS viscous diffusion has been neglected since for most of the boundary layer the magnitude of the SGS viscous diffusion is smaller than the magnitude of the other SGS terms in the energy equation.

The transformation metrics do not have fluctuations and are independent of the filtering operation. However, care must be taken when evaluating the metrics numerically to avoid excessive damping of the spectral components for the Cartesian coordinate system in wave space.[5]

The diffusive fluxes are given by using the chain rule on

$$\widetilde{\sigma}_{ij} = 2\widetilde{\mu}\widetilde{S}_{ij} - \frac{2}{3}\widetilde{\mu}\delta_{ij}\widetilde{S}_{kk}, \qquad \widetilde{q}_j = -\widetilde{k}\frac{\partial \widetilde{T}}{\partial x_j} \ , \quad (16)$$

where $\widetilde{\mu}$ and $\widetilde{k}$ are the viscosity and thermal conductivity corresponding to the filtered temperature $\widetilde{T}$ and their fluctuations are neglected. Vreman *et al.*[10] perform *a priori* tests using DNS data obtained from the calculation of a mixing layer at Mach numbers in the range 0.2–0.6, and concluded that neglecting the nonlinearities of the diffusion terms in the momentum and energy equations is acceptable.

The effect of the subgrid scales along the curvilinear grid lines appears on the right hand side of the governing equations through the SGS stresses τ_{ij}, SGS heat flux $\partial Q_j/\partial\xi_j$, and SGS turbulent diffusion $\partial\mathcal{J}_j/\partial\xi_j$. These quantities are defined as

$$\tau_{ij} = \overline{\rho}\,(\widetilde{u_i u_j'} - \widetilde{u}_i\widetilde{u}_j') \ , \quad (17)$$

$$Q_j = \overline{\rho}\,\left(\widetilde{u_j' T} - \widetilde{u}_j'\widetilde{T}\right) \ , \quad (18)$$

$$\mathcal{J}_j = \overline{\rho}\,\left(\widetilde{u_j' u_k u_k} - \widetilde{u}_j'\widetilde{u_k u_k}\right) \ , \quad (19)$$

The equation of state has been used to express the pressure-velocity correlation appearing in the total energy equation in terms of Q_j.

Subgrid-scale models

The SGS terms are closed using the models described in Martín *et al.*[11] Namely, the one-coefficient dynamic model is used to compute τ_{ij}, the mixed model is used to compute Q_j, and Knight's[12] model is used to compute $\mathcal{J}_j$. These models are composed of a scale-similar and an eddy-viscosity part. In this way, the models reproduce the local energy events that the grid cannot resolve while providing the dissipation that is generally underestimated by purely scale-similar models. The expressions for these models are

$$\begin{aligned} \tau_{ij} &= -C 2\overline{\Delta}^2\overline{\rho}\,|\widetilde{S}'|\left(\widetilde{S}'_{ij} - \frac{\delta_{ij}}{3}\widetilde{S}'_{kk}\right) + \overline{\rho}\,(\widetilde{\widetilde{u}_i\widetilde{u}'}_j - \widetilde{\widetilde{u}}_i\widetilde{\widetilde{u}'}_j) \ , \\ Q_j &= -C\frac{\overline{\Delta}^2\overline{\rho}\,|\widetilde{S}'|}{Pr_T}\frac{\partial\widetilde{T}}{\partial\xi_j} + \overline{\rho}\,\left(\widetilde{\widetilde{u}'_j\widetilde{T}} - \widetilde{\widetilde{u}}'_j\widetilde{\widetilde{T}}\right) \ , \\ \mathcal{J}_j &= 2\widetilde{u}'_k\tau_{jk} \ , \end{aligned} \quad (10)$$

where $\overline{\Delta} = (\overline{\Delta}_\xi\,\overline{\Delta}_\eta\,\overline{\Delta}_\zeta)^{1/3}$, with $\overline{\Delta}_\xi$, $\overline{\Delta}_\eta$ and $\overline{\Delta}_\zeta$ as the grid spacings in the LES grid, $|\widetilde{S}'| = (2\widetilde{S}'_{ij}\widetilde{S}'_{ij})^{1/2}$ and $\widetilde{S}'_{ij}$ is the transformed strain-rate tensor. The expressions for the model coefficients can be found in Martín *et al*,[11] and their extension to curvilinear coordinates is described in Armenio and Piomelli.[13]

Filtering and ensemble averaging

We require two filtering operations to evaluate the mixed models. These operations are performed multiple times to evaluate the smallest resolved scales. Note that $\widehat{\widetilde{f}} = \widehat{\overline{\rho}\,\widetilde{f}}/\widehat{\rho}$ and $\overline{\widetilde{f}} = \overline{\overline{\rho}\,\widetilde{f}}/\overline{\rho}$ represent quantities associated with the test and scale-similar representation of $\widetilde{f}$, respectively. These two filtering operations are in accordance with a second-order discretization to minimize the commutation error between the filtering and differencing operations,[14] and are given by

$$\begin{aligned} \widehat{\widetilde{f}}_i &= \frac{1}{4}\left(\widetilde{f}_{i-1} + 2\widetilde{f}_i + \widetilde{f}_{i+1}\right), \\ \overline{\widetilde{f}}_i &= \frac{1}{8}\left(\widetilde{f}_{i-1} + 6\widetilde{f}_i + \widetilde{f}_{i+1}\right), \end{aligned} \quad (20)$$

where the corresponding filter widths are[15] $\widehat{\Delta}_i = \sqrt{6}\,\overline{\Delta}_i$ and $\overline{\overline{\Delta}}_i = \sqrt{3}\,\overline{\Delta}_i$, with $\overline{\Delta}_i$ being the LES grid spacing. These filtering operations are performed in the computational space, since it takes less computational time than performing the filtering operations in physical space.[5]

To evaluate the model coefficients we use the ensemble-averaging operation $\langle . \rangle$. To preserve Galilean invariance the ensemble-averaging operation is performed after transforming the filtered quantities from the computational to the physical space.[13] Then the ensemble-averaging operation is performed in the streamwise and spanwise directions. Note that for the elliptical cone the flow is not homogeneous in these directions, thus a more sophisticated filtering operation such as Lagrangian filtering should be used in future calculations.

Numerical method

For the convective fluxes we use a fourth-order hybrid finite-difference method.[16] This scheme has low dissipation properties, and was designed to perform DNS and LES of compressible flows. The time advancement technique is based on the DPLU relaxation method of Candler *et al.*[18] and was extended to second-order accuracy by Olejniczak and Candler.[19] The viscous fluxes are evaluated using fourth-order central differences. Finally, the transformation metrics are evaluated using fourth-order central differences so that the inaccuracy of the numerical evaluation of the metrics coefficients is less than the inaccuracy of the convective fluxes.

Validation

To validate the implementation of the SGS models in curvilinear coordinates, we use the *a priori* and *a posteriori* tests in a compressible boundary layer. In the *a priori* test the flow field variables obtained from a DNS are filtered to yield the exact SGS terms, and the filtered quantities are used to asses the accuracy of the parameterization. In the *a posteriori* test, the large, resolved turbulent scales are used to model the SGS terms during a LES.

The flow conditions are $Re_\theta = 7670$, $M_e = 4$, $T_e = 5000$K, $\rho_e = 0.5$ kg/m^3 and Karman number $Ka = 700$, where $Ka = \delta/z_\tau$ is an estimate of the largest to smallest turbulence scales in the flow. The DNS grid is $384 \times 128 \times 128$ grid points in the streamwise, spanwise and wall-normal directions respectively. The homogeneous directions are equispaced and the wall-normal direction is stretched. The domain size is $8\delta \times 2\delta \times 15\delta$ and the domain resolution is $\Delta x^+ = 15$, $\Delta y^+ = 11$ and $0.15 \leq \Delta z^+ \leq 46$ within the boundary layer.[20]

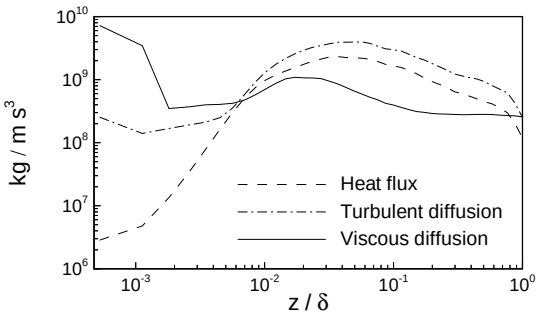

FIGURE 1. Divergence of the SGS terms appearing in the total energy equation for the flat plate boundary layer.

To filter the DNS data and map it onto the LES grid, top-hat filters are applied along the three directions using

$$\overline{f}_i = \frac{1}{2n}\left(f_{i-\frac{n}{2}} + 2\sum_{i-\frac{n}{2}+1}^{i+\frac{n}{2}-1} f_i + f_{i+\frac{n}{2}} \right) , \qquad (21)$$

with $\overline{\Delta}_i = 8\Delta_i$, $\overline{\Delta}_j = 2\Delta_j$, and $\overline{\Delta}_k = 2\Delta_k$, where $\overline{\Delta}_i$ and Δ_i are the LES and DNS grid spacings, respectively. With these filter widths the energy percentage residing in the SGS is up to 20%, and the domain size and resolution are $48 \times 64 \times 64$ and $120\Delta x^+$, $22\Delta y^+$ and $0.30 \leq \Delta z^+ \leq 92$, respectively.

We use supersonic boundary conditions in the free stream and periodic boundary conditions in the streamwise and spanwise directions. Thus, the boundary layer is temporally developing. In low-speed simulations, periodic boundary conditions may not be valid since the amount of kinetic energy in the free stream may not be sufficient to maintain the turbulence levels in the boundary layer. However, this is not an issue in the present simulations, since the kinetic energy in the free stream is substantial. However, an important consideration when performing DNS of temporally developing boundary layers is the growth of the displacement thickness, δ^*, which represents the distance by which the streamlines in the boundary layer edge are shifted due to the temporal development of the boundary layer. Significant growth of δ^* may affect the important flow statistics. Thus, the growth of δ^* in the relevant time scale must be assessed. We find that the growth of δ^* in one $\tau_\tau = \delta/u_\tau$ is less than 8%. Also, the distribution of turbulent kinetic and internal energy within the boundary layer is constant in that time period.

We first consider the results from the *a priori* test. Figure 1 compares the magnitude of the un-

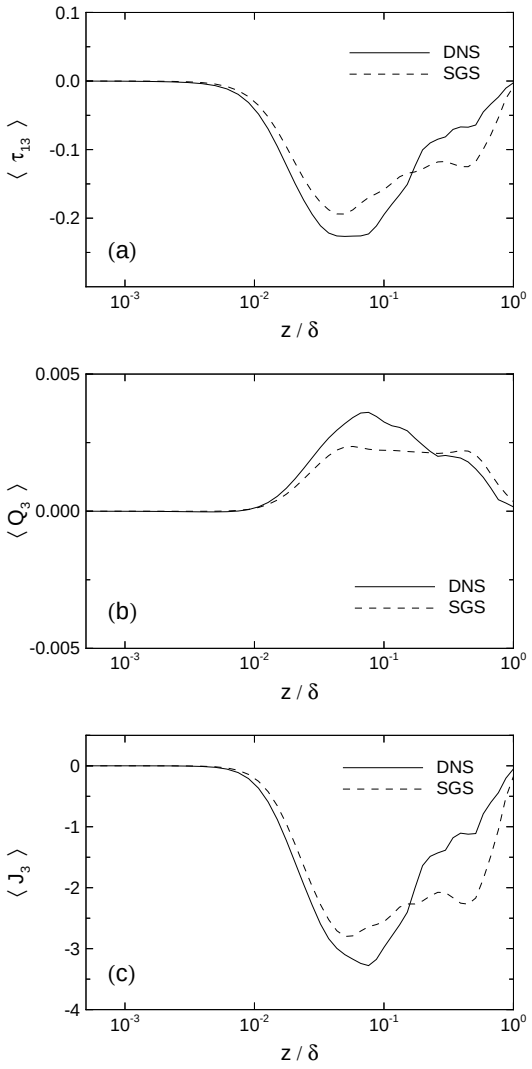

FIGURE 2. *A priori* comparison of the SGS terms for the flat plate boundary layer. The variables are nondimensionalized using τ_w and u_τ given by the DNS.

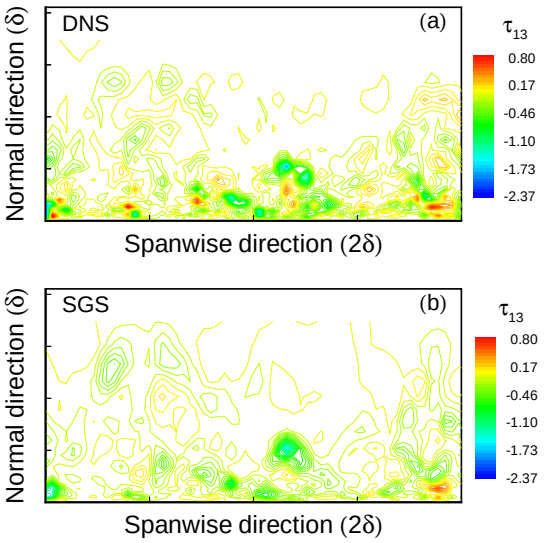

FIGURE 3. *A priori* comparison of the SGS stress τ_{13} for the flat plate boundary layer. The variables are nondimensionalized using τ_w given by the DNS.

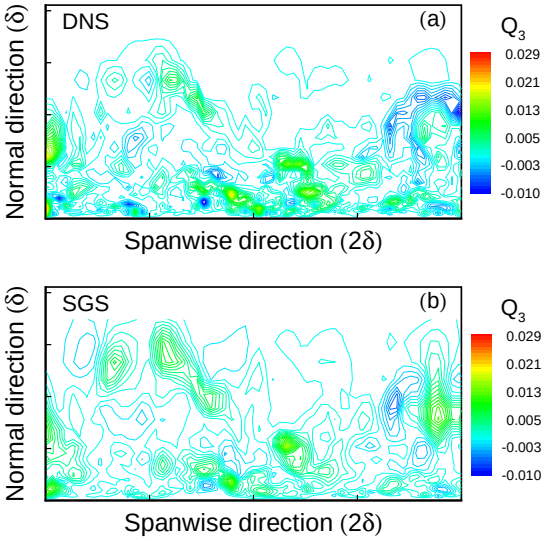

FIGURE 4. *A priori* comparison of the wall-normal SGS heat flux Q_3 for the flat plate boundary layer. The variables are nondimensionalized using τ_w and u_τ given by the DNS.

closed terms appearing in the total energy equation. Throughout most of the boundary layer, the SGS turbulent diffusion and SGS heat flux are the dominant terms. Near the wall, the SGS heat flux is negligible since the flow is adiabatic, and the SGS turbulent diffusion is small since there is little redistribution of turbulent kinetic energy by the SGS. Thus, the SGS viscous diffusion representing the dissipation of kinetic energy into heat due to the SGS turbulent scales is dominant near the wall. However, since the mean viscous diffusion near the wall is substantial, the SGS viscous diffusion can be neglected.

Figure 2 plots the average of the SGS terms across the boundary layer. The global representation of the modeled terms is in good agreement with the DNS. Figures 3 through 5 plot contours of the SGS terms on spanwise planes of data. The magnitude and local features associated with the SGS terms are well represented by the mixed models.

To perform the *a posteriori* test, we advance a LES and a coarse DNS using the same resolution as the LES up to a dimensionless time $tu_{\tau\circ}/\delta_\circ = 1.0$, where $u_{\tau\circ}$ and $\delta_\circ$ are the initial friction velocity and boundary layer thickness. Figure 6 plots the mean velocity profile with Van-Driest transformation for the simulations. The LES agrees very well with the DNS result

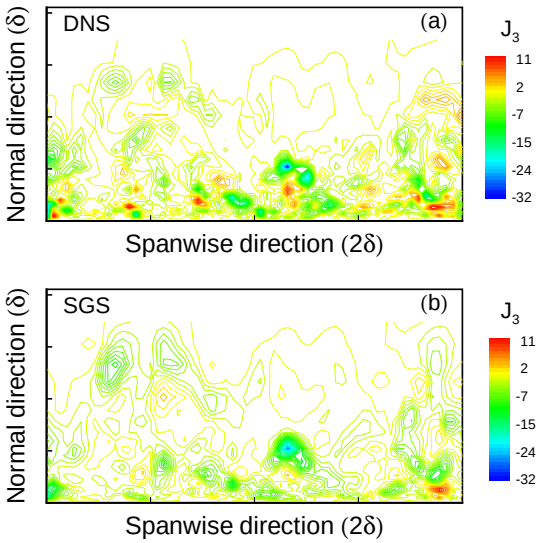

FIGURE 5. *A priori* comparison of the SGS turbulent kinetic energy diffusion $\mathcal{J}_3$ for the flat plate boundary layer. The variables are nondimensionalized using τ_w and u_τ given by the DNS.

and the error is less than 6%. The error for the coarse DNS is up to 20%. Figure 7 plots the friction velocity. Again, the error for the LES is 6%, indicating that the small over-prediction of the transformed velocity is a result of the under-predicted u_τ. However, for the coarse DNS simulation the error in u_τ is 14%, which is larger than the error in the transformed velocity. Thus, the under-estimation in the transformed velocity profile is due to both the low resolution near the wall and the different flow physics in the absence of the small-scale turbulence features.

Elliptic cone flow description

For the purpose of future comparison with experimental data, we chose one of the cone geometries that are being studied at Princeton Gas Dynamics Laboratory Mach 8 Facility.[1] The 2:1 elliptic ratio cone has a nose diameter of $d = 0.08$ mm, length $L = 0.1524$ m, 13.8° half-angle on the major axis, and a zero angle of attack. Surface heat flux and hot-film measurements[2,4] and computational simulations using parabolized stability theory[2,3] have been performed on this geometry.

The flow conditions in the freestream are Mach number $M_\infty = 8$, $T_\infty = 59.02$ K, and $\rho_\infty = 0.512$ kg/m^3. These conditions correspond to a freestream unit Reynolds number $Re_{x,\infty} = 14.2 \times 10^6$ m^{-1} and a total enthalpy $h_\circ = 8.2 \times 10^5$ m^2/s^2. The three dimensionality of the geometry causes a stronger flow compression at the leading edge (major axis) which

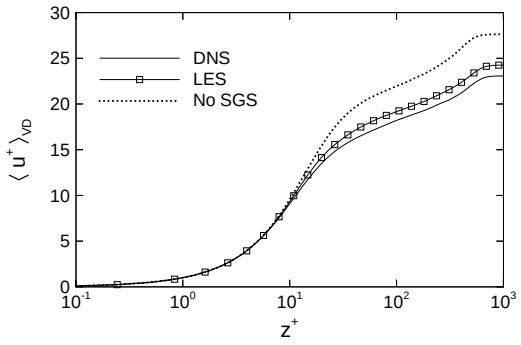

FIGURE 6. *A posteriori* comparison of the mean velocity profile scaled with Van-Driest transformation for the flat plate boundary layer.

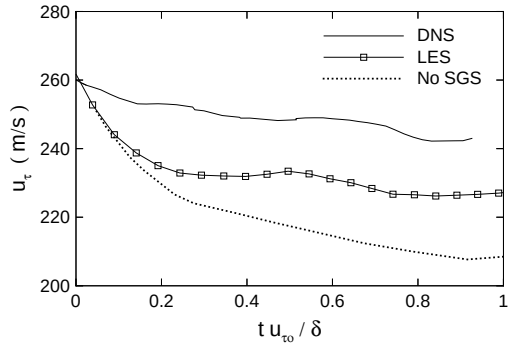

FIGURE 7. *A posteriori* comparison of the friction velocity for the flat plate boundary layer.

leads to crossflow from the leading edge to the centerline (minor axis). Consequently the boundary layer is fattest and thickest at the center line where transition occurs first.[1,2,3,4] Kimmel *et al.*[3] find that the low-momentum flux at the centerline results in an inflectional velocity profile and subsequent early transition. Flow visualization[1] reveals hairpin structures near the centerline region which indicate early stages of transition, and elongated streaks near the off-axis regions that at high Reynolds numbers break down into a series of chain-like structures. Our goal is to provide additional details of the flow phenomena.

Simulation method

The size of the computational domain required to perform a LES on the cone configuration is constrained by the shock-standoff distance and the size of the cone. In the wall normal direction, we need enough grid points to contain the shock. The shock angle is is approximately $\theta_s = 1.2\theta_c$, where θ_s and θ_c are the shock and cone angles respectively. Thus the maximum shock-standoff distance is about 8 mm, roughly two times the boundary layer thickness at the center-

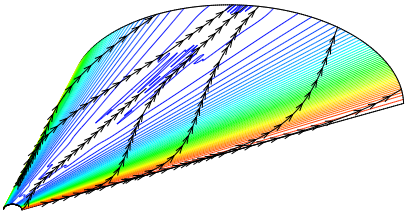

FIGURE 8. Streamlines and density contours for the laminar cone simulation. Note that the contours range from 0.2 to 0.4 kg/m^3 on the surface and from 0.2 to 1.5 kg/m^3 at the exit plane.

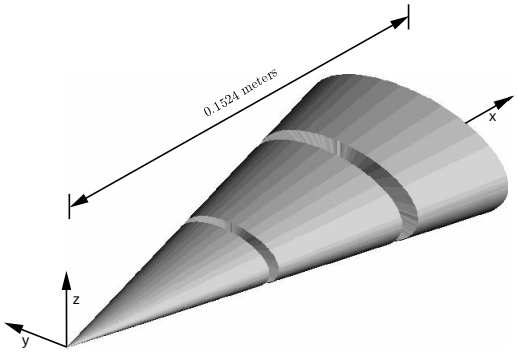

FIGURE 9. Sketch of the elliptic-cone segments for the LES.

line near the end of the cone.[1] Thus, in the wall-normal direction the domain must expand about 3δ from the surface. In the spanwise direction, the largest major axis is about 7.5δ, and the length of the cone is roughly 31δ. Thus, the required computational domain is a rectangular box of dimensions $31\delta \times 17\delta \times 3\delta$ in the streamwise, spanwise and wall-normal directions.

The resolution requirements are determined by the state of the flow which can be estimated by considering the DNS data of a zero-pressure gradient boundary layer at similar conditions. The wall-temperature condition for the cone is nearly adiabatic, the post-shock Mach number number at the edge of the boundary layer is roughly $M_e = 6.8$, and the boundary layer thickness ranges from 3 to 6 mm.[1] These conditions are similar to those of recent DNS of an adiabatic flat plate,[20] where $M_e = 4$ and $\delta = 7$mm. Note that increasing the Mach number decreases the size of the streamwise length scales.[21] Thus in what follows, the resolution requirements in the streamwise direction maybe slightly underestimated. If we neglect the effect of pressure gradients, we can assume that the Karman number for the flat plate and the cone turbulent boundary layers are comparable since the wall temperature and edge conditions are similar. With this assumption, and knowing the required resolution to perform a LES of the flat plate case, we infer that the total number of grid points required to perform a LES over the entire hypersonic elliptical cross-section cone is approximately $186 \times 576 \times 54$ in the streamwise, spanwise and wall-normal directions, respectively. The spacing is uniform in the spanwise and streamwise directions and stretched in the wall-normal direction. This gives a resolution of roughly $\Delta\xi^+ = 117$, $\Delta\eta^+ = 20$ and $0.30 \leq \Delta\zeta^+ \leq 92$ in the streamwise, spanwise and wall-normal directions, respectively. With this grid the boundary layer is well resolved.

To initialize the LES, we use the laminar solution obtained from an implicit blunt-body flow code using a finite-volume technique for the spatial discretization, and a Data-Parallel Line Relaxation (DPLR) method for the time integration.[22] In order to avoid interpolation as much as possible, we use two different grids for the finite-volume (laminar, steady calculation) and the finite-difference (LES) so that the grid-cell centers of the finite-volume grid match the finite-difference grid points in the spanwise and streamwise directions. The flow variables are interpolated in the wall-normal direction ensuring mass conservation. Figure 8 shows the afterbody of the laminar solution. The contours represent density and range from 0.2 to 0.4 kg/m.[3] The streamlines illustrate the crossflow towards the centerline and show that fluid originating at the leading edge coalesces at the centerline farther downstream. The shock location, the laminar boundary layer and the stagnation region at the nose are also accurately predicted.

Future work will involve performing the actual LES of the cone configuration. The size of the cone problem is roughly thirty times larger than that of the zero-pressure gradient boundary layer LES. The most affordable way to compute the hypersonic cone flow configuration is by dividing the cone into segments and performing a LES on each, see Figure 9. The flow is initialized using the results from the laminar calculation with a prescribed freestream disturbance spectrum resembling that present in the experiments. To initialize the flow from one segment to the next, we will use the inflow generation method of Li *et al.*[23] Namely, a time series of instantaneous outflow planes are extracted from the previous segment calculation. Then the signal is made periodic and used as inflow conditions for the next segment as many times as necessary. Li *et al.*[23] tested and validated this method

by comparing the simulation results of a spatially developing turbulent mixing layer to experimental data. Finally, the database obtained from the LES will be compared against experimental data.

Conclusions

In this paper a formulation of subgrid-scale models for compressible flows in generalized curvilinear coordinates has been presented. The implementation of the LES has been validated by comparison against the DNS simulation of a zero-pressure gradient, turbulent boundary layer. From the *a priori* test, it was found that the models give good statistical and local predictions of the turbulent flow. From the *a posteriori* test, we found that using the hybrid finite-difference treatment of the convective fluxes gives a good prediction of the friction velocity and transformed velocity profile.

The simulation method for the elliptic cone geometry has been discussed. The domain size and resolution have been presented. The resulting problem size is thirty times larger than that of the flat plate LES. However, the grid resolution requirements could be relaxed if more information about the transitional and turbulence stages of the flow were known. Namely, it would be beneficial to obtain experimental measurements of the wall unit z_τ at early stages of transition and fully turbulent regimes. In that way, a more appropriate non-uniform streamwise grid spacing could be prescribed. Also, details about the freestream disturbances in the experimental facility and at early stages of transition are desirable to initialize the inflow appropriately and to compare the LES to experimental data. Data provided from experimental flow visualization would be extremely helpful in testing the ability of the current models to reproduce the details of coherent structures. Finally, experimental time evolution information is also desirable to test the evolution of the large-scale turbulence that is predicted by the LES.

Finally, since the flow of interest is not homogeneous, further studies need to be perform to upgrade the calculation of the model coefficients from the ensemble averaging to the Lagrangian procedure. This will involve controlled computational experiments to find the appropriate time scales for each of the SGS terms.

Acknowledgments

We would like to acknowledge the support from the Air Force Office of Scientific Research Grant number No. AF/F49620-98-1-0035. This work was also sponsored by the Army High Performance Computing Research Center under the auspices of the Department of the Army, Army Research Laboratory cooperative agreement number DAAH04-95-2-0003 / contract number DAAH04-95-C-0008, the content of which does not necessarily reflect the position or the policy of the government, and no official endorsement should be inferred. A portion of the computer time was provided by the University of Minnesota Supercomputing Institute. Greg Weirs is supported by the ASCI Flash Center at the University of Chicago under DOE contract B341495.

References

[1] Huntley, M., Wu, P., Miles, R.B., Smits, A.J., "MHZ Rate Imaging of Boundary Layer Transition on Elliptic Cones at Mach 8," *AIAA Paper* 00-0379, January 2000.

[2] Kimmel, R.L., and Poggie, J., "Laminar-Turbulent Transition in a Mach 8 Elliptic Cone Flow," *AIAA Journal,* **37**, 1080, 1999.

[3] Kimmel, R.L., Klein, M.A., and Schwoerke, S.N., "Three-Dimensional Hypersonic Laminar Boundary-Layer Computations for Transition Experiment Design," *Journal of Spacecraft and Rockets,* **34**, 409, 1997.

[4] Poggie, J., Kimmel, R.L., and Schwoerke, S.N., "Traveling Instability Waves in a Mach 8 Flow over an Elliptic Cone," *AIAA Journal,* **2**, 2000.

[5] Jordan, S.A., "A Large-Eddy Simulation Methodology in Generalized Curvilinear Coordinates," *Journal of Computational Physics*, **147**, 322-340, 1999.

[6] Hirsch, C., *Numerical Computation and External Flows*, Wiley, New York, 1991.

[7] Leonard, A., "Energy Cascade in Large-Eddy Simulations of Turbulent Fluid Flows," *Advances in Geophysics*, **18A**, 237, 1974.

[8] Favre, A., "Équations des Gaz Turbulents Compressible. I. Formes Générales," *Journal de Mécanique*, **4**, 361, (1965a).

[9] Favre, A., "Équations des Gaz Turbulents Compressible. II. Méthode des Vitesses Moyennes; Méthode des Vitesses Macroscopiques Pondérées par la Masse Volumique," *Journal de Mécanique*, **4**, 391, (1965b).

[10] Vreman, B., B. Geurts, and H., "Subgrid-modeling in LES of compressible flow," *Applied Scientific Research*, **54**, 191, (1995).

[11] Martín, P.M., U. Piomelli and G.V. Candler, "Subgrid-Scale Models for Compressible Large-Eddy Simulations," *Theoretical and Computational Fluid Dynamics*, Vol. 13, No. 5, Feb. 2000. Also in *Proceedings of the ASME Symposium on Transitional and Turbulent Compressible Flow, Paper No. 99-7313,*

July 1999.

[12] Knight, D., G. Zhou, N. Okong'o, and V. Shukla, "Compressible large eddy simulation using unstructured grids," *AIAA Paper No. 98-0535*, 1998.

[13] Armenio, V., U. Piomelli, and V. Fiorottto, "Applications of a Lagrangian mixed model in generalized coordinates," *Direct and large-eddy simulation III*, edited by P. R. Voke, N. D. Sandham and L. Kleiser, (Kluwer Academic Publishers,Dordrecht), pp. 135-146, (1999).

[14] Ghosal, S., and Moin, P., "The Basic Equations for the Large0Eddy Simulation of Turbulent Flows in Complex Geometry," *Journal of Computational Physics*, **118**, 24-37, 1995.

[15] Lund, T.S., "On the use of discrete filters for large-eddy simulation," *Center for Turbulence Research, Annual Research Briefs*, 1997.

[16] Olejniczak, D.J., V.G. Weirs, J. Liu, and G.V. Candler, "Hybrid finite-difference methods for DNS of compressible turbulent boundary layers," *AIAA Paper No. 96-2086,* June 1996.

[17] Weirs, V.G., and G.V. Candler, "Optimization of weighted ENO schemes for DNS of compressible turbulence," *AIAA Paper No. 97-1940,* July 1997.

[18] Candler, G.V., W.J. Wright, and J.D. McDonald, "Data-Parallel Lower-Upper Relaxation method for reacting flows," *AIAA Journal,* 32, pp. 2380, 1994.

[19] Olejniczak, D.J., and G.V. Candler, "A Data-Parallel LU relaxation method for DNS of compressible flows," *1st International Conference in DNS and LES*, Louisiana, August 1997.

[20]. Martin, M.P., and G.V. Candler, "DNS of a Mach 4 Boundary Layer with Chemical Reactions," *AIAA Paper No. 2000-0399,* January 2000.

[21] Spina, E.F., Donovan, J.F., and Smits, A.J., "On the structure of high-Reynolds-number supersonic turbulent boundary layers," *Journal of Fluid Mechanics*, **222**, 293, 1991.

[22] Wright, M.J., G.V. Candler, and D. Bose, "Data-Parallel Line Relaxation Method for the Navier-Stokes Equations," *AIAA Journal*, Vol. 36, No. 9, pp. 1603-1609, Sep. 1998. Also AIAA Paper No. 97-2046, June 1997.

[23] Li, N., Baralas, E., and Piomelli, U., "Inflow conditions for large-eddy simulations of mixing layers," *Physics of Fluids*, **12**, 935, 2000.